Earth and Planetary Science Letters 616 (2023) 118216

Contents lists available at ScienceDirect

Earth and Planetary Science Letters

journal homepage: www.elsevier.com/locate/epsl

Differences between the central Andean and Himalayan orogenic wedges: A matter of climate

Peter G. DeCelles *, Barbara Carrapa

Department of Geosciences, University of Arizona, Tucson, USA

ARTICLE INFO

Article history:
Received 9 February 2023
Received in revised form 4 May 2023
Accepted 10 May 2023
Available online xxxx
Editor: A. Webb

Keywords:
climate vs. tectonics
Himalaya
Andes
monsoon

ABSTRACT

The Central Andean and Himalayan orogenic belts provide an ideal natural experiment to test the potential role of climate in controlling orogeny. Approximately equal in age and along-strike length, both orogenic wedges are forming in plate-marginal convergent tectonic settings: The Andes in a retroarc setting and the Himalaya in a collisional setting against the Tibetan backstop. The Central Andes orogenic wedge is volumetrically and aerially nearly two times larger than the Himalayan orogenic wedge, despite the Himalaya having accommodated two to three times more tectonic shortening. The Himalaya exports at least four times more sediment owing to much greater erosion rates as signified by widespread Cenozoic metamorphic rocks and very young (<10 Ma) low-temperature thermochronologic ages. The Central Andes are thermochronologically old (mostly >20 Ma), have no exposures of Cenozoic metamorphic rocks, and are mantled by volcanic and sedimentary rocks, attesting to shallow, slow erosion. We conclude that greater intensity of the Indian Monsoon relative to the South American Monsoon since Oligocene time accounts for the differences in orogen size and characteristics. When viewed as an orogenic wedge that has developed largely after formation of the Tibetan orogenic collage, the Himalaya is neither the largest nor hottest among Earth's orogens.

1. Introduction

The effects of climate on orogeny, and *vice versa*, have been debated for decades, with studies supporting opposite ends of the interpretational spectrum (e.g., Dahlen and Suppe, 1988; Molnar and England, 1990; Willett, 1999, 2010; Montgomery et al., 2001; Zeitler et al., 2001; Lamb and Davis, 2003; Meade and Conrad, 2008; Herman et al., 2013; Clift, 2017; Stalder et al., 2020; Wolf et al., 2022). The debate commonly is framed in terms of proxy records of global mountain building and climate trends (e.g., the potential relationship between northern hemisphere glaciation and global orogeny). This approach suffers from ambiguous relationships among proxy records and the great diversity of individual orogenic systems (Willett, 2010). An alternative approach addresses the nature of climate-orogeny dynamics in the context of an individual orogenic belt or a local region within a single orogenic belt, which may produce conflicting results that are difficult to apply on a more general level (Burbank et al., 2003; Wobus et al., 2003). Here we leverage an ongoing natural experiment that allows straightforward assessment of the influence of climate on orogeny in a comparison of the Himalayan and Central Andean orogenic belts. These two fold-thrust belts have equal strike lengths (Fig. 1), were created over the last ~60 million years (Ma) by crustal shortening along convergent plate tectonic boundaries (one subduction-related, the other collisional), and contain most of Earth's highest mountains. Although both are and have been influenced by strongly seasonal climate during much of Cenozoic time, the Himalaya is affected by a much stronger monsoon than the Central Andes. Thus, the two orogens can be compared to assess the effects of differing monsoon intensity. One advantage of this comparison is that the Central Andes and the Himalaya are the two largest, active fold-thrust belts on Earth, sharing the same, exclusive "orogenic weight class" with similar scales and durations.

Stretching more than 7,000 km roughly north-south from equatorial to polar latitudes, the Andes form a prominent orographic barrier between the Pacific Ocean and the South American continent (Figs. 1a, 2a). The Central Andes between ~15°S and ~33°S, contain the highest mountains outside of Asia and the second largest orogenic plateau (the Puna-Altiplano). The Himalaya forms the middle 2,400-km-long sector of the 5,600-km-long composite orogenic system that embraces the northern perimeter of the Indian subcontinent from southern Pakistan to the Irrawaddy delta, and marks the orographic divide between arid central-southern Asia and relatively more humid northern India/Pak-

* Corresponding author.
E-mail address: decelles@arizona.edu (P.G. DeCelles).

https://doi.org/10.1016/j.epsl.2023.118216
0012-821X/

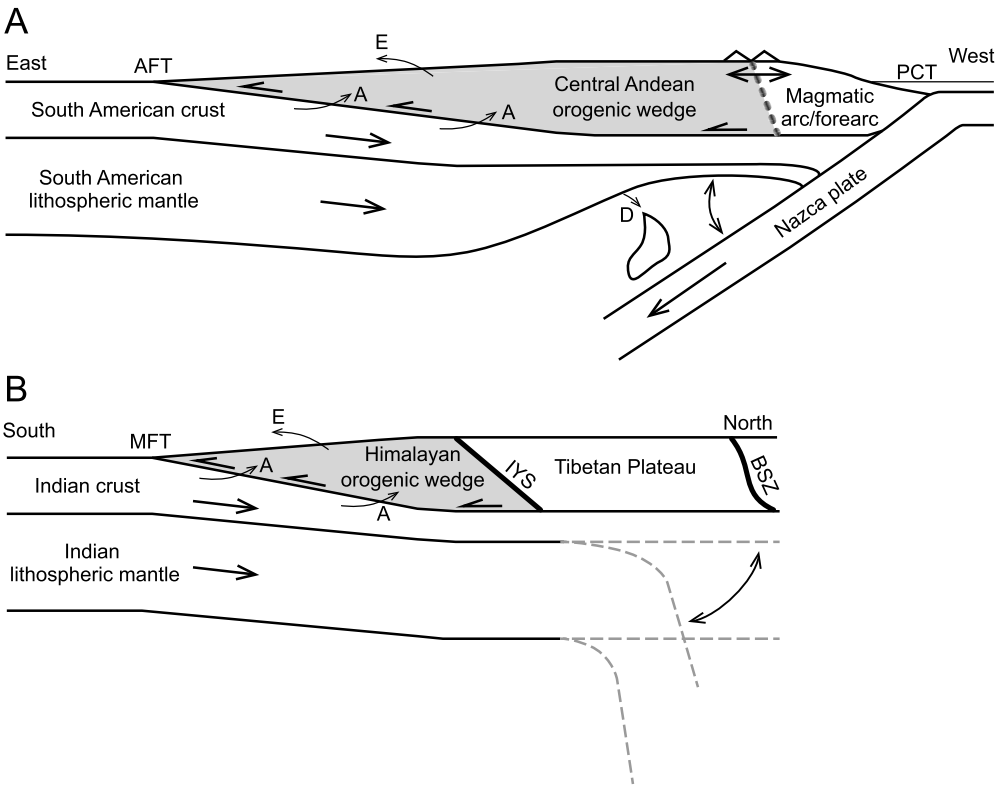

Fig. 1. Schematic lithospheric-scale cross-section of the Central Andean and Himalayan orogenic wedges in their plate tectonic contexts. Gray domains are the orogenic wedges. (A) Central Andean orogen: A, accretion; E, erosion; D, lithospheric delamination/dripping. AFT represents the Andean frontal thrust; PCT is the Peru-Chile trench. (B) Himalayan orogen: MFT, Main Frontal thrust; IYS, Indus-Yarlung suture; BSZ, Bangong suture zone. Double headed arrows in both diagrams indicate ranges of variation in the orientations of the Nazca plate and Indian lower crust/lithosphere.

istan/Nepal/Bhutan (Fig. 1b). Together with the enormous orogenic landmass of the Karakoram and Hindu Kush Ranges and the Tibetan and Pamir Plateaus, the Himalaya is the highest part of the greatest area (~3.2 x 10^6 km^2) of extremely elevated topography on the planet. Although the Himalaya and Central Andes share many characteristics, they differ dramatically in terms of orogenic volumes, total shortening, depth and amount of erosion, and mass export. These differences are most often attributed to contrasting plate tectonic settings (e.g., Wolf et al., 2022), the Andes being a Cordilleran-style orogen formed in response to subduction of the oceanic Nazca plate under westward moving South America, and the Himalaya being the result of a massive intercontinental collision. Although structural and tectonic contrasts between the two are consistent with cordilleran vs. collisional tectonics, we highlight several contrasts in the character of these two orogens that indicate the principal difference between them is the magnitude of erosion, which is controlled mainly by climate.

2. Definitions and terminology

We use the term *orogenic wedge* for the rock mass between the topographic surface and the basal detachment or shear zone, which separates rocks that have been displaced laterally and thickened by folding and thrust faulting—in this case mostly upper crustal sedimentary and igneous/metasedimentary rocks—from lower crustal and lithospheric rocks that have not been as much deformed (i.e., the 'autochthon'). In the Central Andes, the orogenic wedge extends from the Andean magmatic arc to the frontal thrust (locally known as the Mandeyapecua or Andean Frontal thrust; Figs. 1a, 2a); in the Himalaya, the orogenic wedge consists of all rocks between the Indus-Yarlung suture zone and the Main Frontal thrust (Figs. 1b, 2b). Whereas thickening may occur in rocks below the basal detachment, most of this material is shoved beneath the Andean magmatic arc or the Tibetan Plateau where it may be gravitationally removed (Beck et al., 2015) or subducted into the mantle (Replumaz et al., 2010). In neither case is this material part of the orogenic wedge (Fig. 1). Although most of the material in the Central Andean orogenic wedge is accreted from the South American plate (Allmendinger et al., 1997; McQuarrie, 2002; Anderson et al., 2018), the western limit of the orogenic wedge is uncertain because of the presence of the magmatic arc, where magma flux from the mantle may have added significant mass to the rear part of the orogenic wedge (e.g., Ward et al., 2017). Magmatic mass influx may be partially or completely offset by gravitational removal of Rayleigh-Taylor or sheet-form density anomalies (e.g., Beck et al., 2015; Ducea et al., 2021). Equally unconstrained is the potential additive effect of underplating of tectonically ablated forearc material (e.g., Kay et al., 2005) beneath the arc and/or retroarc region. For all these reasons our analysis restricts the western margin of the Andean orogenic wedge to the eastern periphery of the Oligocene-modern magmatic arc (Figs. 1a, 2a). This is a conservative definition because the arc has migrated eastward through time (Kay et al., 2005) into the rear part of the orogenic wedge, which was tectonically thickened during latest Cretaceous-early Cenozoic shortening (e.g., Arriagada et al., 2006; Henriquez et al., 2022). Our analysis does not include this earlier-formed orogenic volume. In the Himalaya, virtually all the material that forms the orogenic wedge has been accreted from the Indian continental plate. The back end of the Himalayan orogenic wedge is clearly marked at the surface by oceanic rocks of the Xigaze accretionary complex in the Indus-Yarlung suture zone (Fig. 1b) (e.g., Burg and Chen, 1984; Yin and Harrison, 2000), and seismic and structural studies suggest the suture dips moderately northward (Gao et al., 2016; Laskowski et al., 2018).

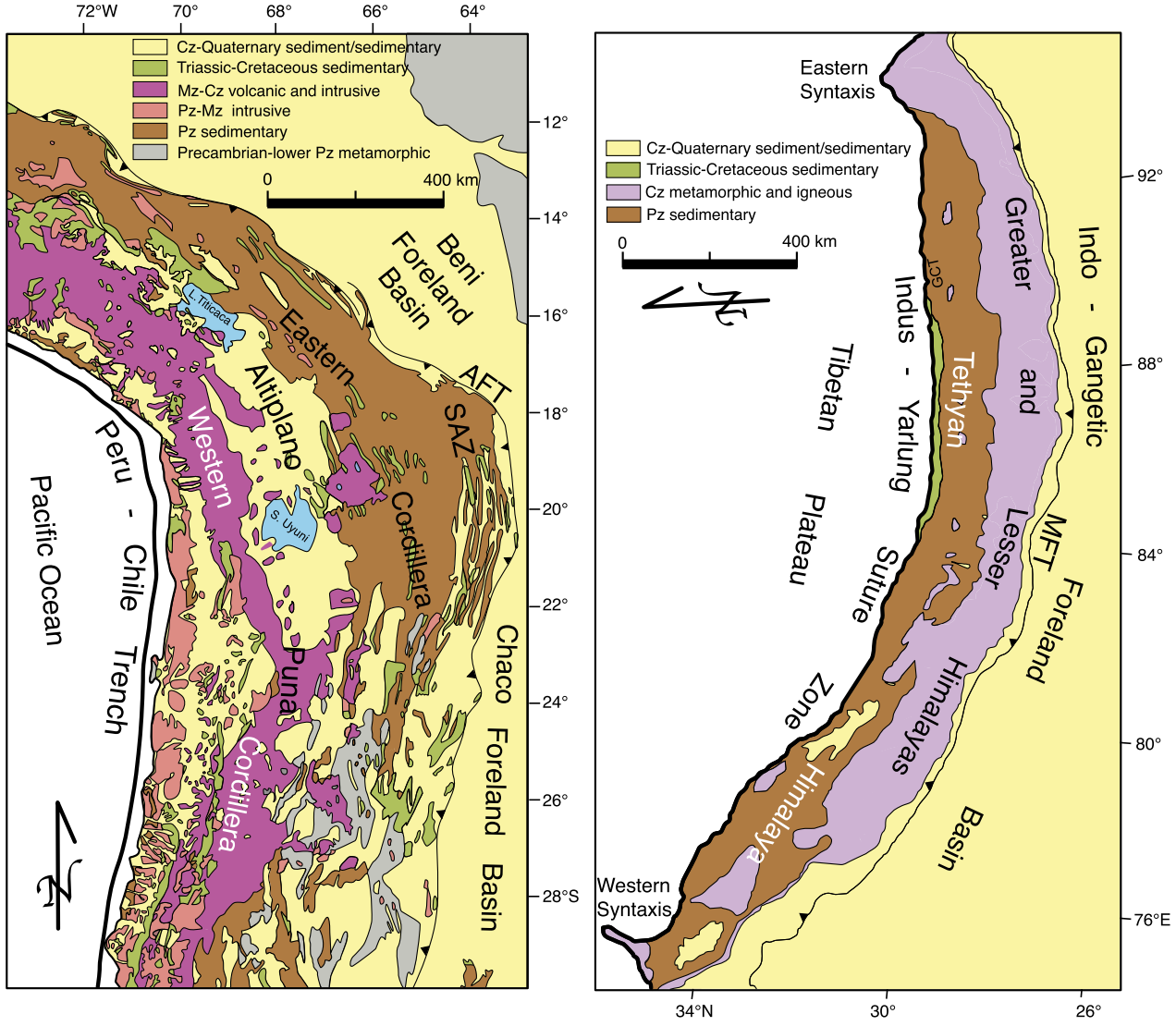

Fig. 2. Simplified geological maps of Central Andean (left, after Schenk et al., 1999) and Himalayan (right, modified from Hodges, 2000) thrust belts at same scale and both verging toward the right for ease of comparison. Barbed lines represent frontal thrust faults on cratonic sides: SAZ is Subandean zone; AFT is Andean Frontal thrust; MFT is Main Frontal thrust. Mapped units are in terms of general rock type, rather than the usual lithostratigraphic units. The Andean thrust belt is dominated by sedimentary and volcanic rocks, whereas the Himalayan thrust belt is composed of approximately 50% high-grade Cenozoic-age metamorphic rocks.

The term *shortening* refers to the distance by which rocks in the orogenic wedge are horizontally shortened by faulting, folding, and penetrative strain. The term *propagation* refers to changes in the length of the orogenic wedge in the shortening direction (DeCelles and DeCelles, 2001); it is an expression of growth of the orogenic wedge. The orogenic wedge grows mainly by *accretion* of new material from below the basal detachment, as the basal thrust/shear zone relocates into previously undeformed rocks (Dahlen and Suppe, 1988). Material is removed from the orogenic wedge by erosion at the upper surface (Fig. 1). Because rocks are deformed (mainly shortened) as they enter the orogenic wedge, total shortening is a measure of how much rock has accreted into the orogenic wedge; erosion is a measure of how much rock has been removed from the upper surface of the wedge.

3. Geological characteristics

3.1. Central Andes

The Andes are the world's longest continuous orogenic belt, forming in response to convergence between the amalgamated cratons of South America and the offshore Peru-Chile trench that marks the eastern surficial edges of the eastward subducting Nazca and Antarctic oceanic plates (Figs. 2a, 3a). The bulk of the Central Andes consists of Neoproterozoic-Cenozoic sedimentary rocks that have been shortened and thickened above the westward underthrusting South American craton (Fig. 2a), in addition to Cenozoic igneous rocks of the magmatic arc (Reutter et al., 2006). The Central Andes have a strike length of ~2500 km and an area of ~1.05 x 10^6 km^2. This region is characterized by an interior ~4,000 m high plateau (Altiplano and Puna) flanked by >6,000 m high Western and Eastern Cordilleras. The Oligocene-present Andean magmatic arc occupies the Western Cordillera and parts of the high plateau between districts to the north (Peru) and south (western central Argentina-Chile) where it has been temporarily extinguished by low-angle subduction (Allmendinger et al., 1997; Ramos, 2009). The Eastern Cordillera is a bivergent thrust system (McQuarrie, 2002; Anderson et al., 2018), and the Subandean zone is an eastward verging fold-thrust belt detached in Silurian shale (Dunn et al., 1995). Surface geology in the Central Andes (Fig. 2a) is dominated by Neogene volcanic rocks (Western Cordillera and Puna), Neoproterozoic-lower Paleozoic sedimentary and igneous

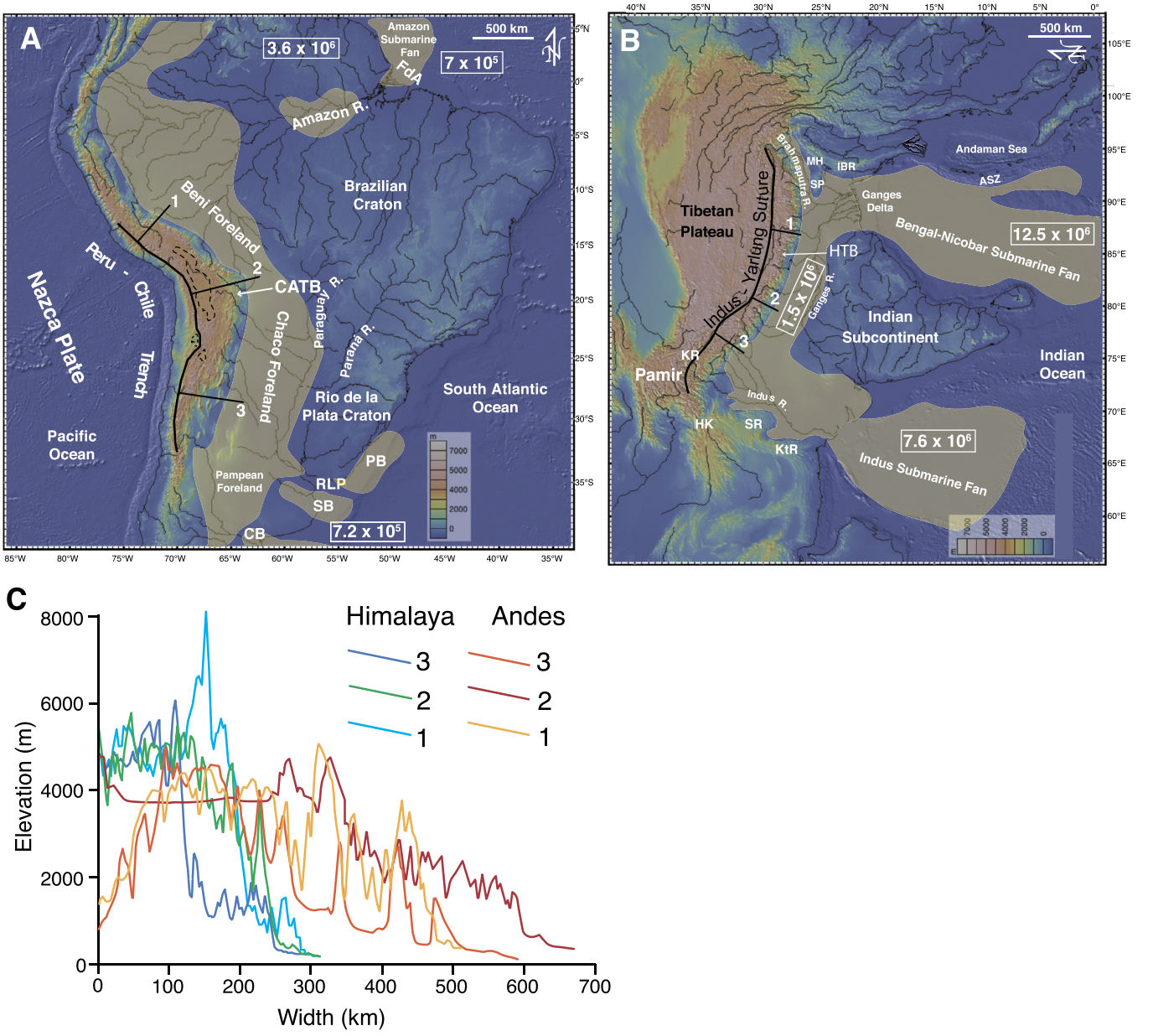

Fig. 3. Digital elevation models (GeoMapApp) of the (A) Central Andean (CATB) and (B) Himalayan (HTB) fold-thrust belts; in this perspective both belts verge toward the right. Bold lines parallel to orogenic belts indicate approximate rear sides of each thrust belt. Lines labeled 1-3 refer to topographic profiles shown in (C). Major accumulations of Cenozoic sediment are indicated by beige regions (from Yrigoyen, 1991; Kingston, 1994; Burbank et al., 1996; Curray et al., 2003; Clift, 2017) and areas enclosed by dashed lines in the Central Andes. Boxed numbers indicate approximate sediment volumes in km^3 for each major sediment reservoir discussed in text. Map A abbreviations: CB, Colorado Basin; FdA, Foz do Amazonas Basin; PB, Pelotas Basin; RLP, Rio de la Plata estuary; SB, Salado Basin. Map B abbreviations: ASZ, Andaman subduction zone; HK, Hindu Kush; IBR, Indo-Burman Range; KR, Karakoram Range; KtR, Kirthar Range; MH, Mikir Hills; SP, Shillong Plateau; SR, Sulaiman Range. (C) Representative topographic profiles transverse to CATB (warm colors) and HTB (cool colors).

rocks (Puna and Eastern Cordillera), and Paleozoic and Cenozoic sedimentary rocks (Eastern Cordillera, Puna-Altiplano, and Subandes) (Allmendinger et al., 1997; McQuarrie, 2002; Reutter et al., 2006). No rocks that were metamorphosed during the Cenozoic orogeny are known to be exposed at the surface in the Central Andes.

Documented tectonic shortening in the Central Andes amounts to as much as ~350 km (McQuarrie, 2002; Anderson et al., 2018; Henriquez et al., 2022) but this is likely a minimum value; the main uncertainties owe to burial of the western part of the thrust belt beneath Neogene volcanic deposits and large sedimentary basins in the Altiplano and Puna, and poor seismic resolution of mid-crustal structure. The maximum east-west span of the Central Andes is ~800 km, in contrast to the narrower and lower Northern and Southern Andes (Montgomery et al., 2001; Ramos, 2009; Horton, 2018). This distance includes the forearc and magmatic arc regions; the orogenic wedge (as defined in Section 2) is approximately 330-540 km wide in the Central Andes. North and south of the Central Andes, total shortening is generally <50 km (Kley and Monaldi, 1998; Horton, 2018). Geodetically measured shortening in the Central Andes is ~9-13 mm/yr (Brooks et al., 2011), and the long-term propagation rate of the Central Andean thrust belt is ~9-10 mm/yr (DeCelles and DeCelles, 2001).

3.2. Himalaya

The Himalaya is a southward verging fold-thrust belt formed by off-scraping of sedimentary, metasedimentary, and igneous rocks from the continental part of the Indian plate (Fig. 1b) (Argand,

1924; Hodges, 2000; Avouac, 2003), which collided with and has been underthrusting the southern part of the Eurasian plate, or a tectonic sliver thereof (Martin et al., 2020), since ca. 60-58 Ma (DeCelles et al., 2014; Hu et al., 2015; Ingalls et al., 2016). The Himalaya is the result of the most recent in a series of intercontinental collisions between fragments of the former supercontinent Gondwana and Eurasia (Şengör et al., 1988; Yin and Harrison, 2000). Tibet-proper, which is the elevated region north of the Indus-Yarlung suture zone (Figs. 1b, 2b), existed as a geological entity with moderately high elevation long before the Indo-Eurasia collision (Murphy et al., 1997; Yin and Harrison, 2000; Kapp and DeCelles, 2019). Although Tibetan crust has thickened and locally shortened during Cenozoic time, the thickening has been accomplished mainly by underthrusting of Indian lower crust that bypasses the Himalayan orogenic wedge (Fig. 1b) and most of the collisional stress has been transmitted to the northern perimeter of Tibet (Murphy et al., 1997; Yin and Harrison, 2000; Kapp and DeCelles, 2019). Tibetan area and volume north of the Indus-Yarlung suture zone, therefore, should not be considered part of the Himalayan orogenic wedge because the processes by which Tibet formed mostly predate the Himalaya. More importantly, apart from relatively minor east-west extension (Yin and Harrison, 2000; Hodges, 2000; Styron et al., 2015), the Himalayan orogenic wedge has not been affected by tectonic processes operating north of the Indus-Yarlung suture zone.

The Himalayan fold-thrust belt encompasses an area of ~5.07 x 10^5 km^2 and has a north-south width ranging between ~250 and 320 km between the Indus-Yarlung suture zone and the topographic front of the range; it is narrowest near the eastern and western syntaxes (Fig. 2b). The suture zone dips moderately northward, such that a portion of the Himalayan orogenic wedge may underlie the southernmost part of the Tibetan Plateau (Gao et al., 2016; Laskowski et al., 2018; Kapp and DeCelles, 2019). The structural geology and stratigraphy of the Himalaya are similar along most of the length of the range (Fig. 2b), with a northern district dominated by Paleozoic sedimentary rocks (the Tethyan Himalayan zone); an axial region composed of amphibolite-facies metasedimentary rocks with Neoproterozoic-Cambrian protolith ages (the Greater Himalayan zone, GHZ); and a southern district composed of mainly Paleo- to Mesoproterozoic low-grade metasedimentary and sedimentary rocks and Cenozoic foreland basin strata (the Lesser and Sub-Himalayan zones) (Robinson et al., 2006; Long et al., 2011; Webb et al., 2011; Martin, 2017; DeCelles et al., 2020). The map shown in Fig. 2b depicts the distribution of rock types, rather than the standard zones, in order to emphasize the widespread metamorphic rocks with predominantly Cenozoic metamorphic ages that occupy approximately 50% of the Himalayan orogenic wedge surface (Hodges, 2000; Kohn, 2014).

The rocks in the Himalayan orogenic wedge have been shortened by 500-900 km since the Early Miocene (DeCelles et al., 2020; Long and Robinson, 2021). Pre-Miocene shortening is sparsely documented but predicted to exceed 300 km based on seismic reflection profiles and balanced cross-sections (Murphy, 2007; Gao et al., 2016). Total Himalayan shortening probably exceeds 1,000 km (Robinson et al., 2006) and is surely underestimated because hanging-wall cutoffs along major thrust faults are generally lost to erosion. Shortening is approximately constant along strike, although it may be less in the east than in the west (Long and Robinson, 2021). The geodetically measured shortening rate in the Himalaya is ~18-20 mm/yr along an azimuth of ~18°N (Wang and Shen, 2020) and the long-term propagation rate of the thrust belt is ~4.5 mm/yr (DeCelles and DeCelles, 2001).

The Himalayan fold-thrust belt is dominated by four major thrust faults/shear zones—the Main Frontal, Main Boundary, Ramgarh, and Main Central thrusts—and a single major extensional shear zone referred to as the South Tibetan detachment system, which is a north-dipping normal fault that forms the boundary between the Greater and Tethyan Himalayan zones. These five fault systems and the rocks they separate can be traced nearly the entire length of the Himalayan fold-thrust belt (Hodges, 2000; Kohn, 2014). Numerous other faults and shear zones are also present.

4. Climate

Climate in both the Central Andes and the Himalaya is strongly seasonal and influenced by warm-season rains (Barnes and Pelletier, 2006; Strecker et al., 2007; Bookhagen and Burbank, 2010; Espinoza et al., 2020). The Indian monsoon, however, produces four to five times greater monthly precipitation than the South American monsoon system in the Central Andes (Bookhagen and Burbank, 2010; Espinoza et al., 2020). Both orogenic sectors have high (>6,000 m) mountains and locally large glaciers, with slightly greater aerial coverage in the Himalaya (~22,800 km^2 [Bolch et al., 2012]) than in the Central Andes (~20,000 km^2 [Masiokas et al., 2020]).

Although paleoclimate reconstructions for both the Central Andes and Himalaya are approximate, the broad paleogeographic constraints suggest that both regions have had strongly seasonal climate since at least 30 Ma: The Central Andes have occupied the subtropics since early Cenozoic time (Müller et al., 2019), and northern continental India was situated ~20°N (Lippert et al., 2014) by ca. 30 Ma. Paleoclimate proxy data suggest that an Indian/Asian monsoon was established by Late Eocene time and may have gradually decreased in intensity since the Early Miocene (Clift et al., 2008; Licht et al., 2014). Fluvial megafans, a characteristic signature of large seasonal fluctuations in fluvial discharge (Leier et al., 2005), have existed in both the Andean and Himalayan foreland basins since Late Eocene (Horton and DeCelles, 2001) and Middle Miocene (DeCelles and Cavazza, 1999), respectively. Evaporative and dry conditions have existed in the Central Andes since at least the Early Miocene (Alonso et al., 1991; Strecker et al., 2007; Quade et al., 2015; Fosdick et al., 2017), and high and dry conditions are documented in southern Tibet since latest Oligocene time (Quade et al., 2020); in both cases this suggests the presence of long-standing orographic rain shadows protecting interior regions of each orogen.

Neither the Central Andean nor Himalayan foreland basin has been strongly influenced by marine conditions since Eocene time, although the Andean foreland was episodically inundated by freshwater to brackish wetlands and lakes during Middle to early Late Miocene time (Hoorn et al., 2010). The Central Andean foreland region has been subject to relatively dry climate and inefficient sediment transport since Eocene time (Fosdick et al., 2017; Folguera and Zárate, 2019; Garzanti et al., 2021). Overall paleogeographic constraints suggest that paleoclimate in northern India has become more seasonal, perhaps with a long-term strengthening of the monsoon to peak intensity during Middle-Late Miocene time (Dettman et al., 2001; Clift et al., 2008), whereas the Central Andes have experienced a weaker monsoon-like climate since the Late Oligocene and a strengthening of Hadley circulation-driven precipitation during the Late Miocene (Carrapa et al., 2019).

5. Erosion and sediment flux

5.1. Central Andes

Topography in the Andes (Fig. 2a) is closely correlated with precipitation and erosion (Montgomery et al., 2001; Barnes and Pelletier, 2006; Strecker et al., 2007). The Andes intersect four global climate zones: (1) In the equatorial intertropical convergence zone, >2 m/yr of precipitation is symmetrically distributed across the range, which is relatively narrow and low; (2) between latitudes

3°S and 15°S, >2 m/yr of rain falls on the eastern side of the orogen while the western side receives an order of magnitude less; (3) the high and wide Central Andes between 15°S and 33°S is in the subtropical desert belt and receives <0.5 m/yr of annual precipitation, which is mainly concentrated on the eastern flank; and (4) south of 33°S in the Westerlies belt, the range narrows again and >2 m/yr of precipitation falls on the western side while the eastern side is relatively dry (Strecker et al., 2007; Garreaud et al., 2009).

River drainage and erosion in the Central Andes are highly asymmetric. At these latitudes, the bulk of the range lies east of the drainage divide, with only 10-30% of the range volume being drained westward, whereas in the Northern and Southern Andes 50-95% of the range volume drains westward (Montgomery et al., 2001). The primary source of water for the Central Andes is the equatorial Atlantic Ocean, but very little water makes it across this sector of the range to the west coast, and the main sediment carrying rivers exit the eastern side of the range (Barnes and Pelletier, 2006) and flow northeastward across the Beni portion of the Amazon basin and southeastward across the Chaco sector of the foreland basin to join the Rio Paraná. The Peru-Chile trench at Central Andean latitudes is sediment-starved (Lamb and Davis, 2003). The Rio Paraná flows south- and southeastward to the coast of Argentina, where it is joined by the Rio Uruguay to form the Rio de la Plata estuary (Fig. 3a). The Amazon River is the world's largest in terms of water discharge, drainage basin area, and total particulate and dissolved loads (1,200 x 10^6 t yr^{-1}) (Milliman and Farnsworth, 2011); it drains the Northern and northern Central Andes, and much of the northern half of the South American continent. Approximately half of the Amazon's sediment load is provided by the northeastward flowing Madeira River, and most of that sediment is derived from the northern half of the Central Andes in Peru and northern Bolivia (Latrubesse and Restrepo, 2014). The Rio Paraná is one of the longest rivers in the world, with a drainage basin area of 2.6 x 10^6 km^2, but it carries a relatively small, mostly fine-grained sediment load (~90 x 10^6 t yr^{-1}) into the Rio de la Plata estuary (Milliman and Farnsworth, 2011; Moreira et al., 2016). Cenozoic sedimentary rocks are widespread across the South American continent, from the Andean foreland basin to the Atlantic coast (Yrigoyen, 1991; Horton, 2018).

Sediment exported from the Andes is stored in three main archives (Fig. 3a): The Amazon submarine fan and adjacent Foz do Amazonas basin, the Rio de la Plata estuary and nearby continental shelf and coastal plain regions, and continental foreland basins directly east of the Andes. The Amazon fan acquires most of its sediment from the Amazon River, occupies an area of 3.3 x 10^5 km^2, is up to ~9 km thick in its proximal part, and contains ~7 x 10^5 km^3 of sediment (Damuth and Flood, 1984). Almost all this sediment was deposited after Middle to Late Miocene time (Damuth and Flood, 1984; Figueredo et al., 2009). Prior to about 11 Ma, the Amazon River was not connected to the Northern and Central Andes, and much of the sediment coming off the orogen was trapped in the continental foreland basin and/or transported northeastward into the Caribbean Sea (Hoorn et al., 2010; Roddaz et al., 2010). Other major basins along the southeastern coast of South America (Salado, Colorado, Rio de la Plata, and Pelotas basins) contain ~7.2 x 10^5 km^3 (Yrigoyen, 1991). Sedimentation in these basins commenced ca. 27 Ma (Folguera and Zárate, 2019), but this southern district of the foreland is dominated by eolian processes today as well as during much of Cenozoic time (Garzanti et al., 2021). The central part of the Andean foreland basin system (between latitudes of 10°S and 35°S) contains ~3.6 x 10^6 km^3 of Cenozoic sediment (Yrigoyen, 1991). Foreland isopach patterns suggest that much greater sediment volume has been eroded from the northern, wetter half of the Central Andean thrust belt, with approximately two-thirds of the total sediment volume stored in the northern foreland (Horton, 2018). A fourth sediment archive in the Central Andes resides within the orogen, embodied by Cenozoic foreland basin deposits that have been incorporated into the thrust belt and large, high-elevation depocenters located mainly in the Altiplano (Figs. 2a, 3a). This material, however, adds to the mass of the central Andean orogenic belt. Altogether, sediment exported from the Central Andes does not exceed ~5.1 x 10^6 km^3. The offshore sediment accumulations (especially the Amazon submarine fan) and Cenozoic basins in eastern Argentina include detritus derived from much of the Andes as well as extra-Andean cratonic uplands, so the actual erosion and sediment yield from the Central Andes alone is likely less than this estimate.

5.2. Himalaya

Topographic profiles of the Himalayan thrust belt exhibit convex- or concave-upward shapes and are strongly coupled to rainfall (Bookhagen and Burbank, 2010). Although Himalayan topography is much steeper than that in the Central Andes, extreme (>6,500 m) elevation is concentrated along a relatively narrow, axial sector of the Himalaya (Fig. 3c).

The Himalaya is drained by three major river systems: the Indus, Ganges, and Brahmaputra (Fig. 3b). The Indus River drains a catchment of 0.97 x 10^6 km^2 that includes the western half of the Indus-Yarlung suture zone and the western third of the Himalayan thrust belt, along with the Karakoram, Hindu Kush, Sulaiman and Kirthar Ranges. The Ganges drains the southern flank of the central Himalaya with tributaries that tap into the northern part of the range, and the Brahmaputra collects the Yarlung River which drains the eastern half of the Indus-Yarlung suture zone and the eastern Himalaya, and rivers flowing northward and westward off the Indo-Burman Range, Shillong Plateau, and Mikir Hills. The Ganges and Brahmaputra Rivers join in Bangladesh and together drain a catchment of 1.6 x 10^6 km^2.

The record of erosion in the Himalaya and surrounding orogenic terrain is archived in the Bengal-Nicobar and Indus submarine fans, in the Ganges and Indus deltas and their prodelta regions, in the continental Indo-Gangetic foreland basin, and in foreland basin and turbidite sequences exposed in the frontal Himalaya and marginal ranges (Fig. 3b) (Einsele et al., 1996; Qayyum et al., 1996; France-Lanord et al., 2016). The Indus fan covers 1.6 x 10^6 km^2 and is up to 9 km thick (Clift et al., 2001). It is fed primarily by the Indus River, with a sediment load of 250 x 10^6 t yr^{-1} (Milliman and Farnsworth, 2011). The Bengal fan has an area of 4 x 10^6 km^2 and maximum sediment thickness estimated at >20 km (Métivier et al., 1999; Curray, 2014; Pickering et al., 2020). It is fed by the combined Ganges and Brahmaputra system with a sediment load of 1,060 x 10^6 t yr^{-1} (Milliman and Farnsworth, 2011).

Clift et al. (2001) estimated the volume of sediment deposited in Indus drainage-related submarine environments (including the Indus fan) since Middle Eocene time at ~7.6 x 10^6 km^3. The Bengal-Nicobar fan has a volume of 12.5 x 10^6 km^3 of which >8 x 10^6 km^3 has accumulated since 20 Ma (Curray, 2014). These estimates are likely minima because large volumes of the eastern part of the Bengal-Nicobar fan have been incorporated into the Andaman subduction zone (Pickering et al., 2020). The Indo-Gangetic foreland basin system contains an additional ~1.5 x 10^6 km^3 (Einsele et al., 1996). Taken together, the continental foreland and submarine fan archives contain >21 x 10^6 km^3 of sediment (Einsele et al., 1996; Métivier et al., 1999; Clift et al., 2001). Although a significant fraction of this sediment could be from southern Tibet and the Karakoram Range (especially in the Indus system; Clift et al., 2001), the moderate regional relief and lack of large erosional canyons in Tibet, together with recent studies suggesting that more than half the present Brahmaputra load comes from a small area around the eastern syntaxis (Stewart et al., 2008), suggest that Ti-

betan input is relatively minor. Similarly, the Indus River derives the bulk of its load from the Himalaya and Karakoram Ranges (Zhou et al., 2020; Feng et al., 2021). The same is true based on the Miocene stratigraphic record of the foreland basin, which contains very little, if any, detritus derived from southern Tibet (Garzanti, 2019). Therefore, most of the sediment flux is derived from the Himalayan fold-thrust belt.

Our estimates are significantly lower than previous estimates of erosional flux from the Himalaya and adjoining areas, as summarized by Ingalls et al. (2016), who calculated a total erosional flux of 50 x 10^6 km^3 from the collision zone, *sensu lato*. A significant fraction of roughly half of the Ingalls et al. estimate, especially that archived in the Makran and Indo-Burman Ranges, could have been derived from areas that are outside of what we consider to be the Himalayan orogenic wedge. Nevertheless, the larger estimates discussed by Ingalls et al. (2016) only exacerbate the issue of 'missing' Himalayan volume, and suggest that the Himalayan orogenic wedge has produced as much as an order of magnitude larger erosional flux than the Central Andes. Tibet, on the other hand, especially its core internally drained region, has been eroded very little. This is shown by widespread flat-lying Cretaceous volcanic rocks, a surface outcrop that is dominated by relatively young sedimentary material and upper Paleozoic-Cenozoic sedimentary rocks (Kapp and DeCelles, 2019), and by relatively old (>45 Ma) low-temperature thermochronological ages (Rohrmann et al. 2012), much like the Altiplano in the Central Andes. The preservation of Tibetan landscapes has been accomplished at the expense of the Himalayan orogenic wedge, which suffers the full erosive force of the Indian monsoon while protecting Tibet.

6. Erosion histories

6.1. Central Andes

The Central Andes exhibit relatively shallow levels of erosion as proxied by low-temperature thermochronometric (apatite and zircon fission-track, and (U-Th)/He) ages. Ages >40 Ma are common in the hinterland region and in isolated uplifts of the Sierras Pampeanas, whereas younger ages (ca. 30-5 Ma) are almost exclusively confined to the Eastern Cordillera and Subandean zones (Fig. 4a; Table S1). The Central Andean hinterland is mainly a receptacle for sediment accumulation, rather than a sediment exporter. Consistent with such low regional erosion rates, the Central Andes contain no surface outcrops of Cenozoic high-grade metamorphic rocks that have been exhumed from great depths (Fig. 2a). The maximum depth of exhumation is ~8-10 km based on low-temperature thermochronology (Stalder et al., 2020), and rocks with Cretaceous-early Paleocene low-temperature cooling ages are widespread (Fig. 4a).

Sandstone petrology and detrital zircon data, together with paleocurrent data, indicate that by Eocene time the Central Andes was an uplifted highland supplying sediment eastward to the foreland basin. Much of the Eocene and younger stratigraphic record of the foreland has been incorporated into the eastward migrating fold-thrust belt. These strata are composed of quartzolithic sands with significant arc-derived components (Horton, 2005, 2018; DeCelles et al., 2011; Amidon et al., 2017; Garzanti et al., 2021). Nowhere in the Cenozoic stratigraphic record of the Central Andes is there a signal of significant erosion of mid-crustal, high-grade metamorphic rocks. Rather, the record indicates derivation from upper crustal rocks, with large recycled sedimentary and volcanic components, consistent with the absence of exposed high-grade metamorphic rocks in the Central Andes (Fig. 2a).

6.2. Himalaya

The rate of erosion in the Himalaya is very rapid, ~1-10 mm/yr depending on location (e.g., Zeitler et al., 2001; Thiede and Ehlers, 2013; Govin et al., 2020). Roughly 50% of the bedrock surface of the Himalaya consists of metasedimentary and metaigneous rocks that experienced amphibolite (and locally granulite to eclogite) facies metamorphism during the Cenozoic orogeny (Fig. 2b). Rocks of the GHZ have metamorphic ages ranging between ~45 and 17 Ma (e.g., Godin et al., 2001; Catlos et al., 2002; Kohn et al., 2005; Martin et al., 2007; Cottle et al., 2009; Tobgay et al., 2012), and low-temperature thermochronometric ages are generally younger than 20 Ma, with most younger than 10 Ma (Fig. 4b; Table S1). Together with thermobarometric data from GHZ metamorphic rocks, this indicates rapid ongoing exhumation from depths exceeding 35 km (Kohn, 2014). Detrital thermochronology indicates that rapid erosion has been ongoing in the Himalaya since late Eocene time (Webb et al., 2017; Clift, 2017; Najman et al., 2019; Stickroth et al., 2019; Feng et al., 2021).

The detrital record of Himalayan erosion stretches back to Paleocene time in early foreland basin deposits along the south side of the Indus-Yarlung suture; Middle Eocene time in the Lesser Himalayan zone; and Middle Miocene in the frontal part of the fold-thrust belt (see review by Garzanti, 2019). A wide array of datasets indicates that the Cenozoic strata were produced by erosion of mainly sedimentary rocks in the Tethyan Himalayan zone and the GHZ. First appearance of metamorphic detritus probably derived from GHZ rocks was between 20 and 12 Ma (see summary in Clift, 2017; Stickroth et al., 2019). Synchronous activity of the Main Central thrust and the South Tibetan detachment helped to exhume GHZ rocks toward the surface, but widespread exposure probably did not occur until Late Miocene time. Major sources of Lesser Himalayan detritus first become prominent from Late Miocene time onward (e.g., Najman et al., 2009).

7. Discussion

7.1. Salient aspects of the argument

Table 1 summarizes key contrasting characteristics of the Central Andean and Himalayan orogenic wedges. Based on input parameters alone (e.g., shortening) the Himalaya would be expected to be at least twice the size of the Central Andes. Average thicknesses of major thrust sheets in the two fold-thrust belts are approximately equal, yet the present volume of the Himalayan orogenic wedge is ~25.8 x 10^6 km^3, and that of the Central Andes is ~43.3 x 10^6 km^3 (Fig. 5). Despite having roughly one-half to one-third the shortening of the Himalaya, the Central Andean orogenic wedge is twice as wide, covers more than twice the area, contains ~25% greater volume between sea-level and the topographic surface and nearly twice as much orogenic wedge volume, and has a propagation rate two to three times that of the Himalaya. The average volumetric growth rate of the Central Andes is 0.72 x 10^6 km^3/Ma, compared to 0.43 x 10^6 km^3/Ma for the Himalaya. The differences in size and growth rate must result from the fact that most (>80%) of the rock that enters the Central Andean orogenic wedge has remained there (Dahlen and Suppe, 1988; DeCelles and DeCelles, 2001; Meade and Conrad, 2008), while a volume of sediment amounting to more than 75% of the rock volume of the present Himalayan orogenic wedge has been eroded from the Himalaya (Einsele et al., 1996; Métivier et al., 1999). Because our analysis is volumetric, it circumvents potential confusion introduced by extraordinary forward propagation of a fold-thrust belt, for example on a very weak basal detachment. The volume (V):shortening (S) ratio of the Central Andes is ~1.4 x 10^5 km^2, whereas this ratio in the Himalaya is ~2.9 x 10^4 km^2.

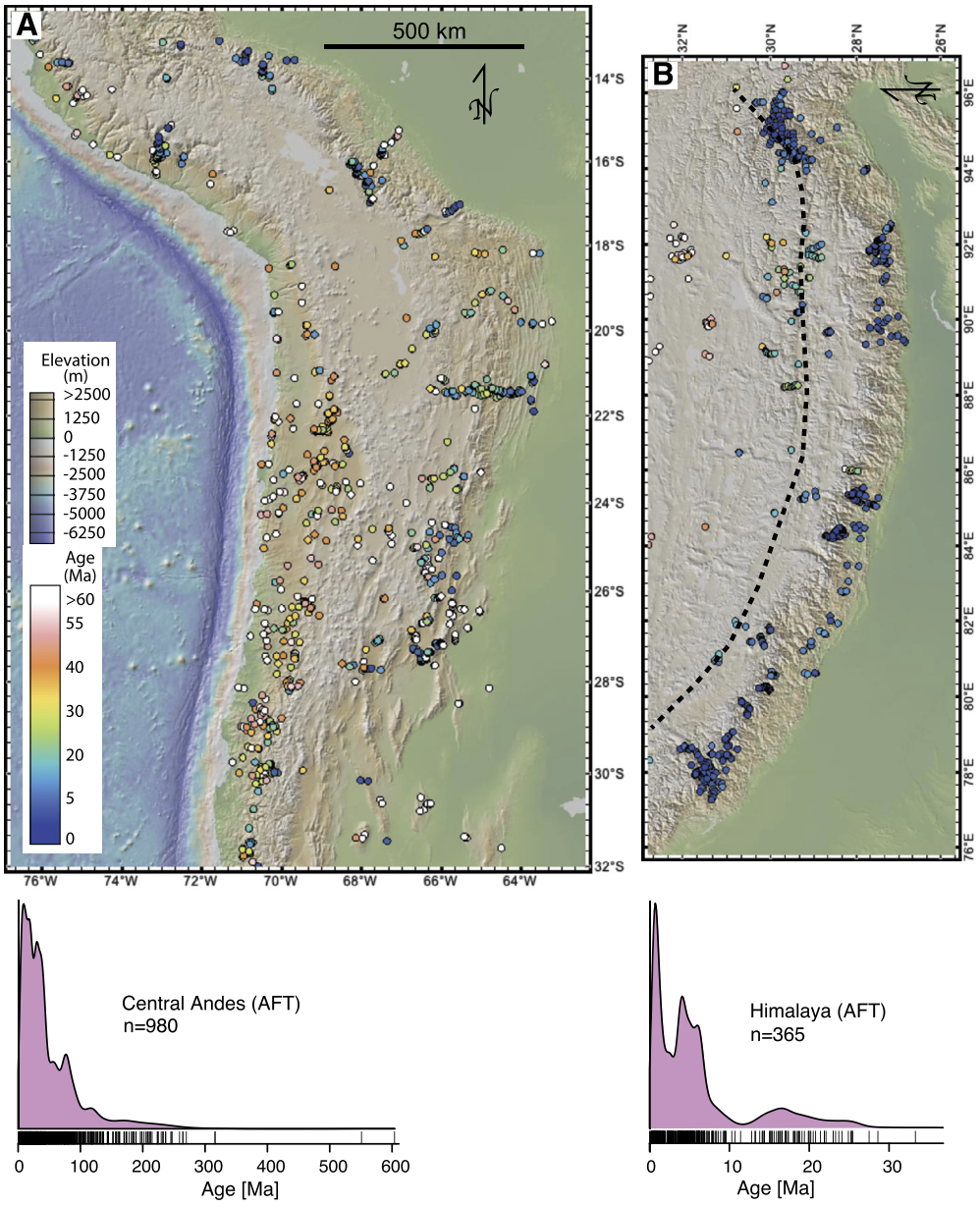

Fig. 4. Apatite fission-track, zircon fission track, and apatite (U-Th)/He ages superimposed on digital elevation models (GeoMapApp) of the (A) Central Andes and (B) Himalaya. Elevation, distance and age scales (shown only in A) are the same for both maps, with dark blue symbols being youngest and brighter colors representing older ages. Dashed line in B represents approximate trace of the Indus-Yarlung suture zone. Below each DEM is the corresponding kernel density estimate of apatite fission track ages; note difference in age scales. Sources of data are provided in Supplementary Table S1.

A first-order approximation of the relative effects of erosion in the Central Andean and Himalayan orogenic wedges can be appreciated using the simple approach outlined in Dahlen and Suppe (1988) and modified to accommodate changes in wedge taper by DeCelles and DeCelles (2001), in which a triangular orogenic wedge is fed by thrust sheets with specified thickness at a rate equal to the shortening rate, and material is extracted from the upper surface of the wedge by erosion. The wedge geometry is characterized by its taper (equal to the sum of the angles of the topographic surface and the basal detachment), which may change through time. The model yields an orogenic wedge width that increases through time, most rapidly during the first 10-20 Ma of growth, and more linearly thereafter (Fig. 6). The parameters that exert strongest control on the shapes of the curves are the shortening rate and the erosion factor, which are proxies for rates of influx and efflux, respectively. Several combinations of shortening rate and erosion factor are shown. Only combinations of relatively rapid shortening (>10 mm/yr) and minimal erosion can produce an orogenic wedge as large as the Central Andean. Conversely, at Himalayan shortening rates, the only way to keep the orogenic wedge from becoming >250 km wide is to have a high erosion factor.

The geological consequences of such divergent rates of erosion are significant and obvious: Nearly 50% of the surface of the Himalayan orogenic wedge is composed of Barrovian metamorphic rocks with Cenozoic metamorphic ages, whereas the Central Andean orogenic wedge has no exposures of such rocks. Instead, the Central Andes are dominated by Cenozoic and older sedimentary and volcanic rocks. In the Himalaya, apart from small extensional basins in the northern part of the belt and frontal wedge-top basins, sediment generally does not accumulate in the steep, rapidly eroding fold-thrust belt (Fig. 2b). Given the input parameters, these differences are difficult to explain with tectonic processes alone and suggest that climate is mainly responsible. A key

Table 1
Key characteristics of Himalayan and Central Andean orogenic wedges. Parenthetical numbers provide sources.

	Shortening (km)	Propagation (km)	Orogenic wedge volume (km^3)	Sediment yield (km^3)	Max. Exhumation depth (km)	Geology	Monsoon rainfall (m/month)
Himalaya	>900 *15-20 mm/yr	250-320 *~4-5 mm/yr	25.8 x 10^6	>21 x 10^6	>35	**>50% Cenozoic metamorphic** **0% volcanic** **<3% Cenozoic sedimentary** 40-50% Paleozoic-Mesozoic sedimentary	0.5-0.8 (1)
Central Andes	≤350 *6-8 mm/yr	>540 *>9 mm/yr	43.3 x 10^6	<5.1 x 10^6	~8 (3)	**0% Cenozoic metamorphic** **>50% Cenozoic sedimentary & volcanic** Up to 30% Neoproterozoic-Mesozoic sedimentary	0.12-0.18 (2)

*Geodetically measured rates of shortening, and average propagation rates based on time of initial shortening.
Sources:
(1) Bookhagen and Burbank, 2010; Leier et al., 2005; (2) Espinoza et al., 2020; (3) Stalder et al., 2020.
See text for all others.

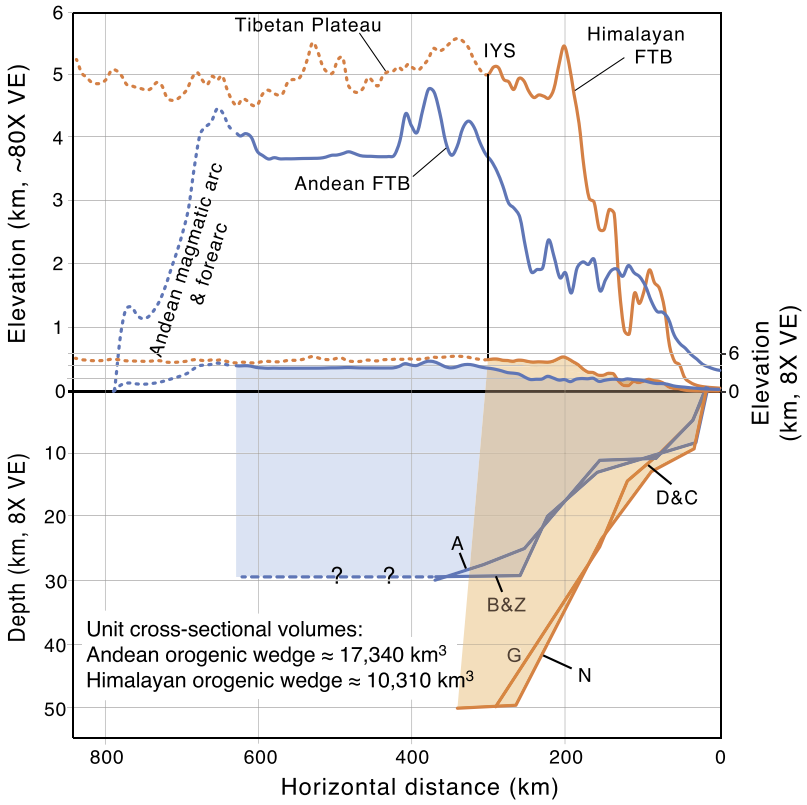

Fig. 5. Orogen-perpendicular topographic profiles (top) and approximate locations of basal detachments (below) for the Central Andean (blue) and Himalayan (orange) fold-thrust belts. Lower panel is vertically exaggerated by a factor of 8; upper two curves in upper panel are vertically exaggerated by a factor of 80; lower two curves in upper panel are at same scale as lower panel (scale on right). Dashed portions of topographic profiles represent parts of each orogen that are not parts of corresponding fold-thrust belts. Shaded areas are used to determine unit cross-sectional volumes for each fold-thrust orogenic wedge. We assume negligible deformation occurs below the basal detachments. Queried dashed line is the poorly documented basal detachment of the Andean orogenic wedge; actual base of the wedge could be deeper. IYS, Indus -Yarlung suture zone; FTB, fold-thrust belt. References for locations of basal detachments abbreviated as follows: A (Anderson et al., 2018), B&Z (Beck and Zandt, 2002), G (Gao et al., 2016), N (Nábělek et al., 2009), D&C (DeCelles and Carrapa, 2021).

point in the argument is that the present conditions of strongly seasonal climates, sediment fluxes, erosion rates, and shortening and propagation rates have existed in the respective orogens since at least 30 Ma, and possibly longer. Finally, the nearly order-of-magnitude difference between Himalayan and Central Andean low-temperature cooling ages is consistent with climatic causes.

The potentially strong control by erosion on orogenic wedge width has been discussed in detail by Dahlen and Suppe (1988), Hilley and Strecker (2004), and Cruz et al. (2010), among others. These studies show that arid climate tends to promote wide orogenic wedges, whereas wetter climates tend to reduce wedge size. Although strongly seasonal climates affect both the Himalaya and Central Andes, the Indian monsoon drops four to five times more precipitation on the southern flank of the Himalaya than the relatively weak South American monsoon system in the Central Andes (Strecker et al., 2007; Bookhagen and Burbank, 2010; Espinoza et al., 2020). The presence of Early Miocene eolian deposits and evaporites in the Central Andes suggests that dry central Andean climate has existed for at least 23 Myr (Alonso et al., 1991; Strecker et al., 2007; Quade et al., 2015; Fosdick et al., 2017; Folguera and Zárate, 2019; Garzanti et al., 2021). As the Central Andes sector of the orogen propagates toward the foreland, the interior of the

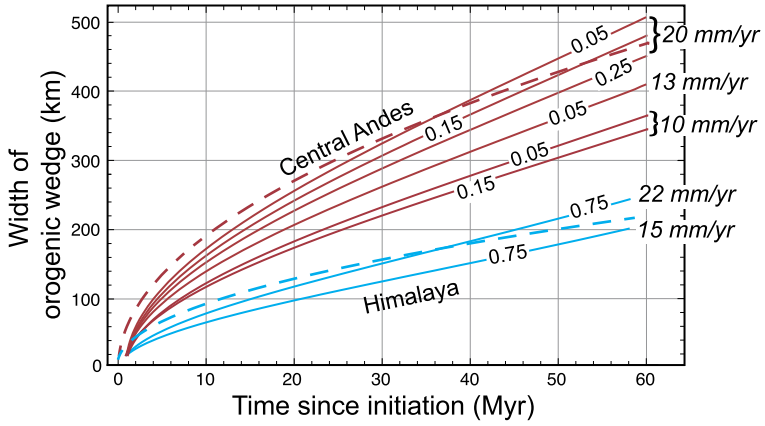

Fig. 6. Graph showing changes in the widths of orogenic wedges (vertical axis) as a function of time since the onset of shortening. Red (Central Andes) and blue (Himalaya) curves are for differing shortening rates as annotated on the right, using the formulation of DeCelles and DeCelles (2001). Variable erosion factors are labeled for each curve. The erosion factor ranges between 0 and 1 and represents the fraction of material that leaves the wedge through time; lower values mean slower erosion. These curves were generated using an average thrust sheet thickness of 10 km and temporally declining taper values of 7° to 5° for the Central Andes and 10° to 6° for the Himalaya. The changing taper has a minor effect. The strongest parameters are shortening rates and erosion factors. The two dashed curves are from the formulation of Dahlen and Suppe (1988) using the following values for the Central Andes: fixed taper = 6°, shortening rate = 20 mm/yr, and erosional factor equivalent to 0.05. Values for the Himalaya curve are: taper = 8°, erosion factor equivalent to 0.25, and shortening rate = 22 mm/yr. Both Dahlen and Suppe (1988) curves are for average thrust sheet thickness of 10 km, Coulomb fracture according to Byerlee's law, and a pore-fluid pressure ratio of 0.7. Note that the gradual flattening of these two curves results from constant taper values.

range becomes increasingly arid, which helps to maintain slow erosion rates (Sobel et al., 2003; Strecker et al., 2007). The contrasts between the Central Andes and Himalaya are consistent with integrated climate-tectonic models for orogenic wedges (e.g., Willett, 1999), in which decreased erosional efficiency promotes orogenic expansion.

7.2. Why standard explanations fail

A standard explanation for differences between Cordilleran and collisional orogenic belts is their obviously contrasting tectonic settings. The widespread distribution of synorogenic high-grade metamorphic rocks observed in some collisional orogens such as the European Alps and the Himalaya (but not in others) is attributed to the abundance of buoyant continental crust in collisional orogenic settings. Cordilleran orogens, on the other hand, involve a relatively easily subducted oceanic plate. In this view, aspects of Cordilleran orogens are often attributed to differences in the age, composition, velocity, structure, and angle of descent of the subducting slab. Whereas we do not discount any of these factors, they cannot explain the differences that we highlight between the Himalaya and the Central Andes because the subducting Nazca slab is completely isolated from the retroarc fold-thrust orogenic wedge, which forms the bulk of the orogen (Fig. 1a). Moreover, major differences in the Andes from north to south (cf. Section 7.3) exist above the same subducting Nazca plate with nearly identical convergence velocities everywhere (e.g., Montgomery et al., 2001; Lamb and Davis, 2003; McGroder et al., 2015). Nor can differences in the composition of the orogenic wedges explain their differences: The bulk of both the Himalayan and Central Andean orogenic wedges consists of sedimentary rocks accreted from the Indian and South American sides of each system, respectively. The Nazca slab provides no material to the Central Andean fold-thrust belt. Although slab descent angle clearly affects the magmatic arc in the Andes, along-strike differences in retroarc shortening and erosion level have no obvious relationship to transient descent angles of the Nazca plate (e.g., Allmendinger et al., 1997; Lamb and Davis, 2003; Horton, 2018). Plate tectonic shortening rates are also not directly relevant in this argument; if they were, the Central Andes might be expected to have much greater shortening than the Himalayan orogenic wedge because the plate convergence rate in the former is twice that of the latter. Instead, Himalayan shortening is more than twice that of the Central Andes. Although not concerned with the issue of along-strike variation in retroarc shortening in the Andes, our analysis is not incompatible with explanations that have been offered (e.g., Allmendinger et al., 1997; Lamb and Davis, 2003; Schellart, 2008; McGroder et al., 2015).

7.3. Why a comparison of the central Andes with northern/southern Andes is not relevant

An argument similar to ours—that erosion is the primary control on orogenic topography—has been used to explain differences between the Central Andes and the relatively narrower, lower, and wetter Northern and Southern Andes (Dahlen and Suppe, 1988; Montgomery et al., 2001; Strecker et al., 2007). Why, then, are the Northern and Southern Andes not more like the Himalaya? The principal differences along strike in the Andes result from contrasting amounts of shortening. The Central Andes have roughly an order of magnitude greater shortening than the Northern and Southern Andes (Kley and Monaldi, 1998; McGroder et al., 2015; Horton, 2018). That the Northern and Southern Andes have little resemblance to the Himalaya is not surprising in view of the 10- to 30-fold greater shortening in the latter. Nevertheless, the fact that the Northern and Central Andes are so different from the Central Andes in terms of both climate and geologic/geomorphic characteristics, while forming on the same tectonic plate in the same Cordilleran tectonic setting, reinforces our basic argument that tectonic setting alone cannot explain the differences in size and composition of the Central Andean and Himalayan orogenic belts. Were it not for rapid erosion in the Himalayan fold-thrust belt, it would be much larger than the Central Andean fold-thrust belt.

7.4. Why the Himalaya has been so erosive for so long

Paleolatitude and climate proxy records (e.g., Strecker et al., 2007; Clift et al., 2008; Lippert et al., 2014) suggest strong seasonality has existed in both the Central Andes and the Himalaya for tens of millions of years, yet the erosional record of the Himalaya is at least four times greater than that of the Central Andes. Why has the Himalaya been so much more erosive than the Central Andes for so long? We suggest this owes to the contrasting geographic settings of the two orogens: the Central Andes are situated along the western margin of South America, 2,800-3,800 km

from the Atlantic Ocean and the source of South American monsoon precipitation, whereas the south-facing Himalaya has been near the Arabian Sea and Bay of Bengal throughout its existence. Marine water occupied the Gangetic foreland basin during Eocene time, and even today the portion of the Himalaya farthest from marine water is only 1,100 km away; most of the eastern two-thirds of the range lies within ~900 km of the Bay of Bengal. Even before the rise of the Himalaya the southern flank of Eurasia was likely subjected to monsoonal climate, again owing to proximity to the Indian (Neotethys) Ocean (Licht et al., 2014) and high topography in the Gangdese magmatic arc along the southern flank of Eurasia (Kapp and DeCelles, 2019). Orography along the southern edge of the Tibetan Plateau has protected it from erosion, much like frontal Subandean and Eastern Cordilleran orography has protected the Central Andean Plateau (Strecker et al., 2007). In this sense, only the rapid rate of tectonic shortening and mass input in the Himalaya are able to sustain orography sufficient to protect Tibet. One implication of this is that if the rate of tectonic growth of the Himalaya begins to significantly decrease, rapid erosion will quickly extend into Tibet-proper. In the Central Andes, where rates of mass influx and shortening are comparatively lower, only an increase in erosional intensity is likely to be capable of strongly diminishing the size of the Central Andean Plateau and orogenic wedge.

7.5. Geodynamic implications

A principal conclusion of our analysis is that the Central Andean fold-thrust belt is Earth's largest coherent orogenic wedge. Since the Himalaya was first interpreted to be a result of intercontinental collision (Argand, 1924), it has been regarded as Earth's greatest orogenic belt, largely on the merits of its extreme topography and relief, which are unequalled anywhere else on the continents. When considered in the context of their associated oceanic trenches, however, Cordilleran orogenic systems routinely exceed Himalayan relief, largely because one plate in a Cordilleran system is oceanic. The Central Andes, for example, fall from a maximum elevation of nearly 7 km to a maximum bathymetric depth of >8 km (Lamb and Davis, 2003). The idea of "Himalayan orogenic exceptionalism" derives from the fact that the Himalaya and Tibet are generally considered together as a contiguous orogenic system, a view that is so widespread and entrenched in geological and geophysical thinking that it could be considered canonical. Countless papers on the tectonics of southern central Asia begin with general statements about the "Himalayan-Tibetan" orogenic system, and many geodynamic modeling efforts aim to build the Tibetan Plateau from near sea-level to its present scale entirely since the onset of the India-Eurasia collision (e.g., Vanderhaeghe, 2012; Wolf et al., 2022). Whereas Tibet and the Himalaya are indeed an integrated topographic mass along with the Karakoram, Pamir, and Hindu Kush Ranges, they are geologically distinct entities and were constructed over nearly mutually exclusive time frames: the Tibetan Plateau mainly before the Cenozoic and the Himalaya entirely during the Cenozoic (Yin and Harrison, 2000; Kapp and DeCelles, 2019). Ongoing subduction, or underthrusting, of India beneath Tibet undoubtedly contributes to Tibetan elevation and lithospheric mass, but the Himalayan fold-thrust belt is made entirely of Indian materials, and what remains of Indian crust below the Himalaya and Tibet largely bypasses, *en route* to the mantle, both the Himalayan orogenic wedge and the part of Tibet that existed prior to the collision (Fig. 1b; e.g., Avouac, 2003; Replumaz et al., 2010). Therefore, from a geodynamic point of view, it makes little sense to model the Himalayan fold-thrust belt as an outcome of processes operating during the growth of Tibet; nor is it logical to use Himalayan geodynamic processes to effect major changes in Tibet, aside from the isostatic effect of shallow subduction of Indian lithosphere.

In turn, this upends the idea that the Himalayan fold-thrust belt, as part of the Himalayan-Tibetan-Pamir "orogen," is Earth's best example of a "large and hot" orogenic system, at the upper end of an evolutionary continuum that begins with "small and cold" orogens like the Pyrenees (e.g., Beaumont et al., 2010; Wolf et al., 2022). When viewed as the separate geological entity that it is, the Himalaya is not particularly large, aside from its exceptionally high elevations; the European Alps are locally wider, and the Zagros and Central Andes both have larger V:S ratios. Nor is the Himalaya especially "hot," insofar as this attribute is based on the abundance of relatively high-temperature Cenozoic metamorphic rocks at the surface. We concur with Clift et al. (2008) that this can be better attributed to the great depth of erosion, with or without assistance from the South Tibetan detachment, rather than a hotter geotherm. Heat flow studies suggest that the Andes are in fact hotter than the Himalaya (Davies, 2013; Lucazeau, 2019). Similarly high-grade metamorphic rocks are presumably present in the middle crust of the Central Andes, where they are expected to remain owing to the low erosion rate unless they are exhumed by syn- or post-orogenic normal faults. This was also the case in the hinterland of the North American Cordilleran thrust belt, where synorogenic high-grade metamorphic rocks of Cretaceous age were not exposed at the surface during construction of the Cordilleran orogenic wedge but were later exhumed in the footwalls of late- to post-orogenic Cenozoic normal faults (e.g., McGrew et al., 2000).

Whereas contrasting tectonic settings can explain the great difference in shortening between the Central Andes and Himalaya, the only logical explanation for the surprisingly small orogenic bulk of the Himalayan fold-thrust belt compared to that of the Central Andes is that the former has been eroding much more rapidly than the latter for most of Neogene time, and the most likely culprit is a stronger monsoon in the Himalaya. Viewing other orogenic belts through the same lens would suggest that dry orogens (such as the Zagros) generally may be expected to be larger than wet orogens of comparable lifespan, even when tectonic variables such as shortening rate might predict the opposite (Dahlen and Suppe, 1988; Hilley and Strecker, 2004).

8. Conclusions

1. When considered as fold-thrust orogenic wedges of approximately the same age, the Central Andes are nearly twice as large as the Himalaya. Tectonic variables such as shortening rate (a proxy for growth rate) predict just the opposite, as the Himalaya has shortened more than three times more than the Central Andes.
2. Rapid erosion of the Himalaya and relatively slow erosion of the Central Andes are indicated by contrasts in sediment efflux, cooling ages, and exposure of mid-crustal rocks at the surface.
3. The differences between the Central Andean and Himalayan orogenic wedges are not explained by tectonic setting or processes, which would predict that the Himalaya should be much larger than the Central Andes. Instead, it is the four- to five-fold greater intensity of the Indian monsoon compared to the South American monsoon that is reducing the bulk of the Himalayan orogenic wedge, while most of the rock that has entered the Central Andean orogenic wedge remains there. That the Indus and Bengal-Nicobar submarine fans date back to Eocene-Oligocene time whereas the Amazon fan dates back to only ca. 11 Ma, along with approximate paleolatitudinal stasis, suggests that this situation has existed in one form or another since Oligocene time.

4. Given the separate geological and geodynamic evolutions of the Himalayan orogenic wedge and the Tibetan Plateau, the two should not be modeled as an integrated orogenic system in which Tibet is born and grows along with the Himalaya. Tibet existed as a complex, multi-stage tectonic collage long before initiation of the Indo-Eurasia collision, and the Himalaya has developed only since that time.

CRediT authorship contribution statement

Peter G. DeCelles: Conceptualization, Funding acquisition, Investigation, Software, Visualization, Writing – original draft, Writing – review & editing. **Barbara Carrapa:** Funding acquisition, Investigation, Visualization, Writing – original draft, Writing – review & editing.

Declaration of competing interest

The authors declare that they have no known competing financial interests or personal relationships that could have appeared to influence the work reported in this paper.

Data availability

Data used to create Fig. 4 are provided in supplementary table S1. All data are published, and the references are provided.

Acknowledgements

S. D. Willett, P. Kapp, M. Blum, F. Ferroni, and C. Howlett provided helpful discussions and comments on earlier drafts of the manuscript. We thank S. George and G. Jepson for help with compiling thermochronological datasets for the Andes and Himalayas, respectively. Insightful reviews by EPSL Associate Editor A.A.G. Webb, P.D. Clift, and G.E. Hilley helped us to significantly improve the manuscript. Funding for this research was provided by National Science Foundation grants EAR-1763432 and EAR-2020935.

Appendix A. Supplementary material

Supplementary material related to this article can be found online at https://doi.org/10.1016/j.epsl.2023.118216.

References

Allmendinger, R.W., Jordan, T.E., Kay, S.M., Isacks, B.L., 1997. Evolution of the Puna-Altiplano plateau of the central Andes. Annu. Rev. Earth Planet. Sci. 25, 139–174.

Alonso, R.N., Jordan, T.E., Tabutt, K.T., Vandervoort, D.S., 1991. Giant evaporite beds of the Neogene central Andes. Geology 19, 401–404.

Amidon, W.H., Luna, L.V., Fisher, G.B., Burbank, D.W., Kylander-Clark, A.R.C., Alonso, R., 2017. Provenance and tectonic implications of Orán group foreland basin sediments, Río Iruyacanyon, NW Argentina (23° S). Basin Res. 29 (S1), 96–112.

Anderson, R.B., Long, S.P., Horton, B.K., Thomson, S.N., Calle, A.Z., Stockli, D.F., 2018. Orogenic wedge evolution of the central Andes, Bolivia (21°S): implications for Cordilleran cyclicity. Tectonics 37, 3577–3609.

Argand, E., 1924. Tectonics of Asia. In: Proc. XIIIth Internat. Geol. Cong., vol. 1, pp. 171–372. Translated by Carozzi, A.V., 1977, Hafner Press, New York, London, 218 pp.

Arriagada, C., Cobbold, P.R., Roperch, P., 2006. Salar de Atacama basin: a record of compressional tectonics in the central Andes since the mid-Cretaceous. Tectonics 25, TC1008. https://doi.org/10.1029/2004TC001770.

Avouac, J.-P., 2003. Mountain building, erosion, and the seismic cycle in the Nepal Himalaya. Adv. Geophys. 46, 1–80. https://doi.org/10.1016/S0065-2687(03)46001-9.

Barnes, J.B., Pelletier, J.D., 2006. Latitudinal variation of denudation in the evolution of the Bolivian Andes. Am. J. Sci. 306, 1–31.

Beaumont, C., Jamieson, R.A., Nguyen, M.H., 2010. Models of large, hot orogens containing a collage of reworked and accreted terranes. Can. J. Earth Sci. 47, 485–515.

Beck, S.L., Zandt, G., 2002. The nature of orogenic crust in the central Andes. J. Geophys. Res. 107, 2230.

Beck, S.L., Zandt, G., Ward, K.M., Scire, A., 2015. Multiple styles and scales of lithospheric foundering beneath the Puna plateau, Central Andes. Geol. Soc. Am. Mem. 212, 43–60.

Bolch, T., Kulkarni Kääb, A., Huggel, C., Paul, F., Cogley, J.G., Frey, H., Kargel, J.S., Fujita, K., Scheel, M., Bajracharya, S., Stoffel, M., 2012. The state and fate of Himalayan glaciers. Science 336, 6079.

Bookhagen, B., Burbank, D.W., 2010. Toward a complete Himalayan hydrological budget: spatiotemporal distribution of snowmelt and rainfall and their impact on river discharge. J. Geophys. Res. 115, F03019.

Brooks, B.A., Bevis, M., Whipple, K., Arrowsmith, J.R., Foster, J., Zapata, T., Kendrick, E., Minaya, E., Echalar, A., Blanco, M., Euillades, P., Sandoval, M., Smalley Jr., R.J., 2011. Orogenic-wedge deformation and potential for great earthquakes in the central Andean backarc. Nat. Geosci. 4, 1–4.

Burbank, D.W., Beck, R.A., Mulder, T., 1996. The Himalayan foreland basin. In: Yin, A., Harrison, T.M. (Eds.), The Tectonic Evolution of Asia. Cambridge University Press, New York, pp. 149–188.

Burbank, D.W., Blythe, A.E., Putkonen, J., Pratt-Sitaula, B., Gabet, E., Oskin, M., Barros, A., Ojha, T.P., 2003. Decoupling of erosion and precipitation in the Himalayas. Nature 426, 652–655.

Burg, J.P., Chen, G.M., 1984. Tectonics and structural zonation of southern Tibet, China. Nature 311, 219–223. https://doi.org/10.1038/311219a0.

Carrapa, B., Clementz, M., Feng, R., 2019. Ecological and hydroclimate responses to strengthening of the Hadley circulation in South America during the Late Miocene cooling. Proc. Natl. Acad. Sci. USA.

Catlos, E.J., Harrison, T.M., Manning, C.E., Grove, M., Rai, S.M., Hubbard, M.S., Upreti, B.N., 2002. Records of the evolution of the Himalayan orogen from in situ Th–Pb ion microprobe dating of monazite: eastern Nepal and western Garhwal. J. Asian Earth Sci. 20, 459–479.

Clift, P.D., 2017. Cenozoic sedimentary records of climate-tectonic coupling in the Western Himalaya. Prog. Earth Planet. Sci. 4, 39.

Clift, P.D., Hodges, K., Heslop, D., Hannigan, R., Hoang, L.V., Calves, G., 2008. Greater Himalayan exhumation triggered by early Miocene monsoon intensification. Nat. Geosci. 1, 875–880.

Clift, P.D., Shimizu, N., Layne, G.D., Blusztajn, J.S., Gaedicke, C., Schluter, H.U., 2001. Development of the Indus Fan and its significance for the erosional history of the western Himalaya and Karakoram. Geol. Soc. Am. Bull. 113, 1039–1051.

Cottle, J.M., Searle, M.P., Horstwood, M.S.A., Waters, D.J., 2009. Timing of midcrustal metamorphism, melting, and deformation in the mount Everest region of southern Tibet revealed by U(-Th)-Pb geochronology. J. Geol. 117, 643–664. https://doi.org/10.1086/605994.

Cruz, L., Malinski, J., Wilson, A., Take, W.A., Hilley, G., 2010. Erosional control of the kinematics and geometry of fold-and-thrust belts imaged in a physical and numerical sandbox. J. Geophys. Res. 115, B09404.

Curray, J.R., 2014. The Bengal depositional system: from rift to orogeny. Mar. Geol. 352, 59–69.

Curray, J.R., Emmel, F.J., Moore, D.G., 2003. The Bengal fan: morphology, geometry, stratigraphy, history and processes. Mar. Pet. Geol. 19, 1191–1223.

Dahlen, F.A., Suppe, J., 1988. Mechanics, growth, and erosion of mountain belts. Spec. Pap., Geol. Soc. Am. 218, 161–178.

Damuth, J.E., Flood, R., 1984. Morphology, sedimentation processes and growth pattern of the Amazon deep-sea fan. Geo Mar. Lett. 3, 109–117.

Davies, J.H., 2013. Global map of solid Earth surface heat flow. Geochem. Geophys. Geosyst. 14, 4608–4622. https://doi.org/10.1002/ggge.20271.

DeCelles, P.G., Kapp, P., Gehrels, G.E., Ding, L., 2014. Paleocene–Eocene foreland basin evolution in the Himalaya of southern Tibet and Nepal: implications for the age of initial India-Asia collision. Tectonics 33, 824–849.

DeCelles, P.G., Carrapa, B., Horton, B.K., Gehrels, G.E., 2011. Cenozoic foreland basin system in the central Andes of northwestern Argentina: implications for Andean geodynamics and modes of deformation. Tectonics 30, TC6013. https://doi.org/10.1029/2011TC002948.

DeCelles, P.G., Carrapa, B., Ojha, T.P., Gehrels, G.E., Collins, D., 2020. Structural and Thermal Evolution of the Himalayan Thrust Belt in Midwestern Nepal. Geol. Soc. Am. Spec. Pap., vol. 547. Geol. Soc. Am, Boulder.

DeCelles, P.G., Carrapa, B., 2021. Coupled rapid erosion and foreland sedimentation control orogenic wedge kinematics in the Himalayan thrust belt of central Nepal. J. Geophys. Res., Solid Earth 126, e2020JB021256. https://doi.org/10.1029/2020JB021256.

DeCelles, P.G., Cavazza, W., 1999. A comparison of fluvial megafans in the Cordilleran (Late Cretaceous) and modern Himalayan foreland basin systems. Geol. Soc. Am. Bull. 111, 1315–1334.

DeCelles, P.G., DeCelles, P.C., 2001. Rates of shortening, propagation, underthrusting, and flexural wave migration in continental orogenic systems. Geology 29, 135–138.

Dettman, D.L., Kohn, M.J., Quade, J., Ryerson, F.J., Ojha, T.P., Hamidullah, S., 2001. Seasonal stable isotope evidence for a strong Asian monsoon throughout the past 10.7 m.y. Geology 29, 31–34.

Ducea, M.N., Chapman, A.D., Bowman, E., Balica, C., 2021. Arclogites and their role in continental evolution, part 2: relationship to batholiths and volcanoes, density and foundering, remelting and long term storage in the mantle. Earth-Sci. Rev. 214C, 103476.

Dunn, J.F., Hartshorn, K.G., Hartshorn, P.W., 1995. Structural styles and hydrocarbon potential of the Subandean thrust belt of southern Bolivia. In: Tankard, A.J., Suarez, S., Welsink, H.J. (Eds.), Petroleum Basins of South America: Am. Assoc. Petrol. Geol. Mem., vol. 62, pp. 523–543.
Einsele, G., Ratschbatcher, L., Wetzel, A., 1996. The Himalaya-Bengal fan denudation-accumulation system during the past 20 Ma. J. Geol. 104, 163–184.
Espinoza, J.C., Garreaud, R., Poveda, G., Arias, P.A., Molina-Carpio, J., Masiokas, M., Viale, M., Scaff, L., 2020. Hydroclimate of the Andes part I: main climatic features. Front. Earth Sci. 8, 64.
Feng, H., Lu, H., Carrapa, B., Clift, P.D., 2021. Erosion of the Himalaya-Karakoram recorded by Indus fan deposits since the Oligocene. Geology 49, 1126–1131.
Figueredo, J., Hoorn, C., van der Ven, P., Soares, E., 2009. Late Miocene onset of the Amazon River and the Amazon deep-sea fan: evidence from the Foz do Amazonas basin. Geology 37, 619–622.
Folguera, A., Zárate, M., 2019. Late Oligocene to Quaternary tectonic evolution of the extra-Andean basins of the Pampean plain, Argentina. J. South Am. Earth Sci. 94, 102207.
Fosdick, J.C., Reat, E.J., Carrapa, B., Ortiz, G., Alvarado, P.M., 2017. Retroarc basin reorganization and aridification during Paleogene uplift of the southern central Andes. Tectonics 36, 493–514.
France-Lanord, C., Spiess, V., Klaus, A., Schwenk, T., 2016. Expedition 354 scientists. In: Bengal Fan. Proceedings of the International Ocean Discovery Program, International Ocean Discovery Program. College Station, TX.
Gao, R., Lu, Z., Klemperer, S.L., Wang, H., Dong, S., Li, W., Li, H., 2016. Crustal-scale duplexing beneath the Yarlung Zangbo suture in the western Himalaya. Nat. Geosci. B, 555–560.
Garreaud, R.D., Vuille, M., Compagnucci, R., Marengo, J., Villalba, R., Grosjean, M., Kiefer, T., 2009. Present-day South American climate. Palaeogeogr. Palaeoclimatol. Palaeoecol. 281, 180–195.
Garzanti, E., 2019. The Himalayan Foreland basin from collision onset to the present: a sedimentary–petrology perspective. Geol. Soc. (Lond.) Spec. Publ. 483.
Garzanti, E., Capaldi, T., Vezzoli, G., Limonta, M., Sosa, N., 2021. Transcontinental retroarc sediment routing controlled by subduction geometry and climate change (Central and Southern Andes, Argentina). Basin Res. 33, 3406–3437.
Godin, L., Parrish, R.R., Brown, R.L., Hodges, K.V., 2001. Crustal thickening leading to exhumation of the Himalayan metamorphic core of central Nepal: insight from U-Pb geochronology and 40Ar/39Ar thermochronology. Tectonics, 729–747. https://doi.org/10.1029/2000TC001204.
Govin, G., van der Beek, P., Najman, Y., Millar, I., Gemignani, L., Huyghe, P., Dupont-Nivet, G., Bernet, M., Mark, C., Wijbrans, J., 2020. Early onset and late acceleration of rapid exhumation in the Namche Barwa syntaxis, eastern Himalaya. Geology 48, 1139–1143.
Henriquez, S., DeCelles, P.G., Carrapa, B., Hughes, A.N., 2022. Kinematic evolution of the central Andean retroarc thrust belt in northwestern Argentina and implications for coupling between shortening and crustal thickening. Geol. Soc. Am. Bull. 134.
Herman, F., Seward, S., Valla, P.G., Carter, A., Kohn, B., Willett, S.D., Ehlers, T.A., 2013. Worldwide acceleration of mountain erosion under a cooling climate. Nature 504.
Hilley, G.E., Strecker, M.R., 2004. Steady state erosion of critical Coulomb wedges with applications to Taiwan and the Himalaya. J. Geophys. Res. 109, B01411. https://doi.org/10.1029/2002JB002284.
Hodges, K.V., 2000. Tectonics of the Himalaya and southern Tibet from two perspectives. Geol. Soc. Am. Bull. 112, 324–350. https://doi.org/10.1130/0016-7606(2000)112<324:TOTHAS>2.0.CO;2.
Hoorn, C., Wesselingh, F.P., ter Steege, H., Bermudez, M.A., Mora, A., Sevink, J., Sanmartin, I., Sanchez-Meseguer, A., Anderson, C., Figueiredo, J.P., Jaramillo, C., Riff, D., Negri, F.R., Hooghiemstra, H., Lundberg, J., Stadler, T., Sarkinen, T., Antonelli, A., 2010. Amazonia through time: Andean uplift, climate change, landscape evolution, and biodiversity. Science 330, 927–931.
Horton, B.K., 2005. Revised deformation history of the central Andes: inferences from Cenozoic foredeep and intermontane basins of the Eastern Cordillera, Bolivia. Tectonics 24, TC3011. https://doi.org/10.1029/2003TC001619.
Horton, B.K., 2018. Sedimentary record of Andean mountain building. Earth-Sci. Rev. 178, 279–309.
Horton, B.K., DeCelles, P.G., 2001. Modern and ancient fluvial megafans in the foreland basin system of the central Andes, southern Bolivia: implications for drainage network evolution in fold-thrust belts. Basin Res. 13, 43–63.
Hu, S., Garzanti, E., Moore, T., Raffi, I., 2015. Direct stratigraphic dating of India-Asia collision onset at the Selandian (middle Paleocene, 59 ± 1 Ma). Geology 43, 859–862.
Ingalls, M., Rowley, D.B., Currie, B., Colman, A.S., 2016. Large-scale subduction of continental crust implied by India-Asia mass-balance calculation. Nat. Geosci. 9, 848–853. https://doi.org/10.1038/NGEO2806.
Kapp, P., DeCelles, P.G., 2019. Mesozoic–Cenozoic geological evolution of the Himalayan-Tibetan orogen and working tectonic hypotheses. Am. J. Sci. 319, 159–254.
Kay, S.M., Godoy, E., Kurtz, A., 2005. Episodic arc migration, crustal thickening, subduction erosion, and magmatism in the south-central Andes. Geol. Soc. Am. Bull. 117, 67–88.
Kingston, J., 1994. Undiscovered petroleum of southern South America. U.S. Geol. Surv. Open-File Rep. 94-559, 443 pp.
Kley, J., Monaldi, C.R., 1998. Tectonic shortening and crustal thickness in the Central Andes: how good is the correlation? Geology 26, 723–726.
Kohn, M.J., 2014. Himalayan metamorphism and its tectonic implications. Annu. Rev. Earth Planet. Sci. 42, 381–419.
Kohn, M.J., Wieland, M.S., Parkinson, C.D., Upreti, B.N., 2005. Five generations of monazite in Langtang gneisses: implications for chronology of the Himalayan metamorphic core. J. Metamorph. Geol. 23, 399–406. https://doi.org/10.1111/j.1525-1314.2005.00584.x.
Lamb, S., Davis, P., 2003. Cenozoic climate change as a possible cause for the rise of the Andes. Nature 425, 792–797.
Laskowski, A.K., Kapp, P., Cai, F., 2018. Gangdese culmination model: Oligocene–Miocene duplexing along the India-Asia suture zone, Lazi region, southern Tibet. Geol. Soc. Am. Bull. 130, 1355–1376. https://doi.org/10.1130/B31834.1.
Latrubesse, E.M., Restrepo, J.D., 2014. Sediment yield along the Andes: continental budget, regional variations, and comparisons with other basins from orogenic mountain belts. Geomorphology 216, 225–233.
Leier, A., DeCelles, P.G., Pelletier, J., 2005. Mountains, monsoons, and megafans. Geology 33, 289–292.
Licht, A., et al., 2014. Asian monsoons in a late Eocene greenhouse world. Nature 513, 501–506.
Lippert, P.C., van Hinsbergen, D.J.J., Dupont-Nivet, G., 2014. Early Cretaceous to present latitude of the central proto–Tibetan Plateau: a paleomagnetic synthesis with implications for Cenozoic tectonics, paleogeography, and climate of Asia. Spec. Pap., Geol. Soc. Am. 507, 1–21.
Long, S., McQuarrie, N., Tobgay, T., Rose, C., Gehrels, G., Grujic, D., 2011. Tectonostratigraphy of the Lesser Himalaya of Bhutan: implications for the along-strike stratigraphic continuity of the northern Indian margin. Geol. Soc. Am. Bull. 123, 1406–1426.
Long, S., Robinson, D.M., 2021. Construction of the Lesser Himalayan–Subhimalayan thrust belt: the primary driver of thickening, exhumation, and high elevations in the Himalayan orogen since the middle Miocene. Geology 49, 1283–1286.
Lucazeau, F., 2019. Analysis and mapping of an updated terrestrial heat flow data set. Geochem. Geophys. Geosyst. 20, 4001–4024. https://doi.org/10.1029/2019GC008389.
Martin, A.J., 2017. A review of Himalayan stratigraphy, magmatism, and structure. Gondwana Res. 49, 42–80.
Martin, A.J., Gehrels, G.E., DeCelles, P.G., 2007. The tectonic significance of (U, Th)/Pb ages of monazite inclusions in garnet from the Himalaya of central Nepal. Chem. Geol. 244, 1–24. https://doi.org/10.1016/j.chemgeo.2007.05.003.
Martin, C.R., Jagoutz, O., Upadhyay, R., Royden, L.H., Eddy, M.P., Bailey, E., Nichols, C.I.O., Weiss, B.P., 2020. Paleocene latitude of the Kohistan–Ladakh arc indicates multistage India–Eurasia collision. Proc. Natl. Acad. Sci. 117 (47), 29487–29494. www.pnas.org/cgi/doi/10.1073/pnas.2009039117.
Masiokas, M.H., Rabatel, A., Rivera, A., Ruiz, L., Pitte, P., Ceballos, J.L., Barcaza, G., Soruco, A., Bown, F., Berthier, E., Dussaillant, I., MacDonell, S., 2020. A review of the current state and recent changes of the Andean cryosphere. Front. Earth Sci. 8, 99.
McGrew, A., Wright, J., Peters, M.T., 2000. Thermobarometric constraints on the tectonothermal evolution of the East Humboldt Range metamorphic core complex, Nevada. Geol. Soc. Am. Bull. 112, 45–60.
McGroder, M.F., Lease, R.O., Pearson, D.M., 2015. Along-strike variation in structural styles and hydrocarbon occurrences, Subandean fold-and-thrust belt and inner foreland, Colombia to Argentina. Geol. Soc. Amer. Mem. 212, 79–113. https://doi.org/10.1130/2015.1212(05).
McQuarrie, N., 2002. The kinematic history of the central Andean fold-thrust belt, Bolivia: implications for building a high plateau. Geol. Soc. Am. Bull. 114, 950–963.
Meade, B.J., Conrad, C.P., 2008. Andean growth and the deceleration of South American subduction: time evolution of a coupled orogen-subduction system. Earth Planet. Sci. Lett. 275, 93–101.
Métivier, F., Gaudemer, Y., Tapponnier, P., Klein, M., 1999. Mass accumulation rates in Asia during the Cenozoic. Geophys. J. Int. 137, 280–318.
Milliman, J.D., Farnsworth, K.L., 2011. River Discharge to the Coastal Ocean: a Global Synthesis. Cambridge University Press, Cambridge.
Molnar, P., England, P., 1990. Late Cenozoic uplift of mountain ranges and global climate change: chicken or egg? Nature 346, 29–34.
Montgomery, D.R., Balco, G., Willett, S.D., 2001. Climate, tectonics, and the morphology of the Andes. Geology 29, 579–582.
Moreira, D., Simionato, C.G., Dragani, W., Cayocca, F., Tejedor, M.L.C., 2016. Characterization of bottom sediments in the Río de la Plata Estuary. J. Coast. Res. 32, 1473–1494.
Müller, R.D., Zahirovic, S., Williams, S.E., Cannon, J., Seton, M., Bower, D.J., Tetley, M.G., Heine, C., Le Breton, E., Liu, S., Russell, S., Yang, T., Leonard, J., Gurnis, M., 2019. A global plate model including lithospheric deformation along major rifts and orogens since the Triassic. Tectonics 38, 1884–1907.
Murphy, M.A., Yin, A., Harrison, T.M., Dürr, S.B., Chen, Z., Ryerson, F.J., Kidd, W.S.F., Wang, X., Zhou, X., 1997. Did the Indo-Asian collision alone create the Tibetan Plateau? Geology 25, 719–722. https://doi.org/10.1130/0091-7613(1997)025<0719:DTIACA>2.3.CO;2.

Murphy, M.A., 2007. Isotopic characteristics of the Gurla Mandhata metamorphic core complex: implications for the architecture of the Himalayan orogen. Geology 35, 983–986.
Nábělek, J.L., Hetényi, J.G., Vergne, J., Sapkota, S., Kafle, B., Jiang, M., Su, H., Chen, J., Huang, B.-S., Hi-Climb Team, 2009. Underplating in the Himalaya-Tibet collision zone revealed by the Hi-CLIMB experiment. Science 325, 1371–1374.
Najman, Y., Bickle, M., Garzanti, E., Pringle, M., Barfod, D., Brozovic, N., Burbank, D., Ando, S., 2009. Reconstructing the exhumation history of the Lesser Himalaya, NW India, from a multitechnique provenance study of the foreland basin Siwalik Group. Tectonics 28 (TC5018). https://doi.org/10.1029/2009TC002506.
Najman, Y., Mark, C., Barfod, D.N., Carter, A., Parrish, R., Chew, D., Gemignani, L., 2019. Spatial and temporal trends in exhumation of the Eastern Himalaya and syntaxis as determined from a multitechnique detrital thermochronological study of the Bengal fan. Geol. Soc. Am. Bull. 131, 1607–1622.
Pickering, K.T., Pouderoux, H., McNeill, L.C., Backman, J., Chemale, F., Kutterolf, S., Milliken, K., Mukoyoshi, H., Henstock, T.J., Stevens, D.E., Parnell, C., Dugan, B., 2020. Sedimentology, stratigraphy and architecture of the Nicobar fan (Bengal–Nicobar fan system), Indian Ocean: results from International Ocean Discovery Program Expedition 362. Sedimentology 67, 2248–2281.
Qayyum, M., Niem, A.R., Lawrence, R.D., 1996. Newly discovered Paleogene deltaic sequence in Katawaz basin, Pakistan, and its tectonic implications. Geology 24, 835–838.
Quade, J., Leary, R., Dettinger, M.P., Orme, D., Krupa, A., DeCelles, P.G., Kano, A., Kato, H., Waldrip, R., Huang, W., Kapp, P., 2020. Resetting southern Tibet: the serious challenge of obtaining primary records of paleoaltimetry. Glob. Planet. Change 191, 103194.
Quade, J., Dettinger, M.P., Carrapa, B., DeCelles, P., Murray, K.E., Huntington, K.A., Cartwright, A., Canavan, R.R., Gehrels, G., Clementz, M., 2015. The growth of the central Andes 22–26°S. Geol. Soc. Am. Mem. 212, 277–308.
Ramos, V.A., 2009. Anatomy and global context of the Andes: main geologic features and the Andean orogenic cycle. Geol. Soc. Am. Mem. 204, 31–65.
Replumaz, A., Negredo, A.M., Guillot, S., Villaseñor, A., 2010. Multiple episodes of continental subduction during India/Asia convergence: insight from seismic tomography and tectonic reconstruction. Tectonophysics 483, 125–134.
Reutter, K.J., Charrier, R., Götze, H.J., Schurr, B., Wigger, P., Scheuber, E., Giese, P., Reuther, C.-D., Schmidt, S., Rietbrock, A., Chong, G., Belmonte-Pool, A., 2006. The Salar de Atacama basin: a subsiding block within the western edge of the Altiplano-Puna plateau. In: Oncken, O., et al. (Eds.), The Andes—Active Subduction Orogeny. Springer, Berlin, pp. 303–325.
Robinson, D.M., DeCelles, P.G., Copeland, P., 2006. Tectonic evolution of the Himalayan thrust belt in western Nepal: implications for channel flow models. Geol. Soc. Am. Bull. 118, 865–885.
Roddaz, M., Hermoza, W., Mora, A., Baby, P., Parra, M., Christophoul, F., Brusset, S., Espurt, N., 2010. Cenozoic sedimentary evolution of the Amazonian foreland basin system. In: Hoorn, C., Wesselingh, F.P. (Eds.), Amazonia, Landscape and Species Evolution: A Look into the Past. Wiley-Blackwell, Chichester, UK, pp. 61–88.
Rohrmann, A., Kapp, P., Carrapa, B., Reiners, P.W., Guynn, J., Ding, L., Heizler, M., 2012. Thermochronologic evidence for plateau formation in central Tibet by 45 Ma. Geology 40, 187–190. https://doi.org/10.1130/G32530.1.
Schellart, W.P., 2008. Overriding plate shortening and extension above subduction zones: a parametric study to explain formation of the Andes mountains. Geol. Soc. Am. Bull. 120, 1441–1454. https://doi.org/10.1130/B26360.1.
Schenk, C., Vigar, R.J., Anderson, C.P., 1999. Maps showing geology, oil and gas fields, and geologic provinces of the South America region. USGS Open-File Report 97-470-D.
Şengör, A.M.C., Altiner, D., Cin, A., Ustaömer, T., Hsü, K.J., 1988. Origin and assembly of the Tethyside orogenic collage at the expense of Gondwana-land. Geol. Soc. (Lond.) Spec. Publ. 37, 119–181.
Sobel, E.R., Hilley, G.E., Strecker, M.R., 2003. Formation of internally drained contractional basins by aridity-limited bedrock incision. J. Geophys. Res. 108 (B7), 2344.
Stalder, N.F., Herman, F., Fellin, M.G., Coutand, I., Aguilar, G., Reiners, P.W., Fox, M., 2020. The relationships between tectonics, climate and exhumation in the Central Andes (18–36°S): evidence from low-temperature thermochronology. Earth-Sci. Rev. 210, 103276.
Stewart, R.J., Hallet, B., Zeitler, P.K., Malloy, M.A., Allen, C.M., Trippett, D., 2008. Brahmaputra sediment flux dominated by highly localized rapid erosion from the easternmost Himalaya. Geology 36, 711–714.
Stickroth, S.F., Carrapa, B., DeCelles, P.G., Gehrels, G.E., Thomson, S.N., 2019. Tracking the growth of the Himalayan fold-and-thrust belt from lower Miocene foreland basin strata: Dumri Formation, western Nepal. Tectonics 38, 3765–3793. https://doi.org/10.1029/2018TC005390.
Strecker, M.R., Alonso, R.N., Bookhagen, B., Carrapa, B., Hilley, G.E., Sobel, E.R., Trauth, M.H., 2007. Tectonics and climate of the southern central Andes. Annu. Rev. Earth Planet. Sci. 35, 747–787.
Styron, R., Taylor, M., Sundell, K., 2015. Accelerated extension of Tibet linked to the northward underthrusting of Indian crust. Nat. Geosci. 8, 131–134. https://doi.org/10.1038/ngeo2336.
Thiede, R.C., Ehlers, T.A., 2013. Large spatial and temporal variations in Himalayan denudation. Earth Planet. Sci. Lett. 371, 278–293.
Tobgay, T., McQuarrie, N., Long, S., Kohn, M.J., Corrie, S.L., 2012. The age and rate of displacement along the main central thrust in the western Bhutan Himalaya. Earth Planet. Sci. Lett. 319–320, 146–158. https://doi.org/10.1016/j.epsl.2011.12.005.
Vanderhaeghe, O., 2012. The thermal–mechanical evolution of crustal orogenic belts at convergent plate boundaries: a reappraisal of the orogenic cycle. J. Geodyn. 56–57, 124–145.
Wang, M., Shen, Z.-K., 2020. Present-day crustal deformation of continental China derived from GPS and its tectonic implications. J. Geophys. Res., Solid Earth 125, e2019JB018774.
Ward, K.M., Delph, J.R., Zandt, G., Beck, S.L., Ducea, M.N., 2017. Magmatic evolution of a Cordilleran flare-up and its role in the creatin of silicic crust. Sci. Rep. 7, 9047. https://doi.org/10.1038/s41598-017-09015-5.
Webb, A.A.G., Yin, A., Harrison, T.M., Célérier, J., Gehrels, G.E., Manning, C.E., Grove, M., 2011. Cenozoic tectonic history of the Himachal Himalaya (north-western India) and its constraints on the formation mechanism of the Himalayan orogen. Geosphere 7, 1013–1061.
Webb, A.A.G., Guo, H., Clift, P.D., Husson, L., Müller, T., Costantino, D., Yin, A., Xu, Z., Cao, H., Wang, Q., 2017. The Himalaya in 3D: slab dynamics controlled mountain building and monsoon intensification. Lithosphere. https://doi.org/10.1130/L636.1.
Willett, S.D., 1999. Orogeny and orography: the effects of erosion on the structure of mountain belts. J. Geophys. Res. 104, 28957–28981.
Willett, S.D., 2010. Late Neogene erosion of the Alps: a climate driver? Annu. Rev. Earth Planet. Sci. 38, 409–435.
Wobus, C.W., Hodges, K.V., Whipple, K.X., 2003. Has focused denudation sustained active thrusting at the Himalayan topographic front? Geology 31, 861–864.
Wolf, S., Huismans, R.S., Braun, J., Yuan, X., 2022. Topography of mountain belts controlled by rheology and surface processes. Nature 606, 516–521.
Yin, A., Harrison, T.M., 2000. Geologic evolution of the Himalayan-Tibetan orogen. Annu. Rev. Earth Planet. Sci. 28, 211–280.
Yrigoyen, M.R., 1991. Energy resources map of the Circum-Pacific region, southeast quadrant. U.S. Geol. Surv. Circum-Pacific Map Series, Map CP-39, scale 1:10,000,000.
Zeitler, P.K., Koons, P.O., Bishop, M.P., Chamberlain, C.P., Craw, D., Edwards, M.A., Hamidullah, S., Qasim Jan, M., Asif Khan, M., Umar Khan Khattak, M., Kidd, W.S.F., Mackie, R.L., Meltzer, A.S., Park, S.K., Pecher, A., Poage, M.A., Sarker, G., Schneider, D.A., Seeber, L., Shroder, J.F., 2001. Crustal reworking at Nanga Parbat: metamorphic consequences of thermal-mechanical coupling facilitated by erosion. Tectonics 20, 712–728.
Zhou, P., Carter, A., Li, Y., Clift, P.D., 2020. Slowing rates of regional exhumation in the western Himalaya: fission track evidence from the Indus Fan. Geol. Mag. 157, 848–863.